Journal of The Electrochemical Society, **160** (6) F514-F521 (2013)
0013-4651/2013/160(6)/F514/8/$31.00 © The Electrochemical Society

An Experimental Study of Polymer Electrolyte Fuel Cell Operation at Sub-Freezing Temperatures

Jeffrey Mishler,[a] Yun Wang,[a,*,z] Roger Lujan,[b] Rangachary Mukundan,[b,*] and Rodney L. Borup[b,*]

[a]*Renewable Energy Resources Lab, Department of Mechanical and Aerospace Engineering, The University of California Irvine, Irvine, California 92697-3975, USA*
[b]*Los Alamos National Laboratory (LANL), Los Alamos, New Mexico 87545, USA*

The ability of polymer electrolyte fuel cells (PEFCs) to startup at subfreezing temperatures is governed by whether it is able to overcome the freezing point (0°C) before product ice prevents the electrochemical reactions. In this work, we experimentally investigated the coulombs of charge Q_c transferred in PEFCs under subfreezing operation before the output voltage drops to 0.0 V. PEFCs with various membranes and catalyst-layer thicknesses, ionomer-carbon ratios, operating current density, and initial hydration of PEFCs were studied, and their influences on cold-start performance and coulombs of charge were experimentally measured. We find that subfreezing temperature, ionomer-catalyst ratio, and catalyst-layer thickness, significantly affect the amount of charge transferred before operational failure, whereas the membrane thickness and initial hydration level have limited effect for the considered cases.
© 2013 The Electrochemical Society. [DOI: 10.1149/2.051306jes] All rights reserved.

Manuscript submitted January 4, 2013; revised manuscript received February 22, 2013. Published March 13, 2013.

Owing to their high efficiency and low emissions, polymer electrolyte fuel cells (PEFC) have received considerable attention for transportation and portable applications. In 2009 alone, about 24,000 fuel cells were shipped. In the US, currently there are over 200 fuel-cell vehicles and 20 buses that are being deployed.[1] The ability of PEFCs to start up at subfreezing temperatures is imperative for their use as a fuel conversion device in transportation applications. Specifically, there are many areas of the world that exhibit subfreezing temperatures for part of a year, and potential automobiles need to be able to start in these conditions. During fuel cell operation water is produced at the cathode electrode and may freeze in the fuel cell, as shown in Figure 1, resulting in reduced electrochemical surface area, hindered reactant transport, and ultimately loss of voltage and power. The technical targets set by the Department of Energy (DOE) is the ability of the fuel cell stack to reach 50% rated power in 30 seconds starting from −20°C, and an unassisted start-up temperature as low as −40°C.[2] The DOE target is to achieve a life time of 5000-hour durability by 2015 with 60% efficiency for transportation and must include freeze starts.[1]

Research is ongoing on the effect of repeated cold starts on fuel cell durability.[1,3] Different GDL and MEA types exhibited different amounts of degradation, with reinforced membranes exhibiting less.[4] Both Mishler et al.[3] and Oberholzer et al.[5] visualized ice formation using high-resolution neutron imaging, and indicated that ice accumulates in MEAs and GDLs. Mishler et al.[3] show that ice formation in the cathode catalyst layer (CL) may be the major reason for cell voltage drop, and validated model predictions using their experimental data, in terms of voltage evolution. Oberholzer et al. showed that water in a condensed phase was observed in the MEA, in the cathode GDL at −15°C, and in the cathode gas channels at −10°C.[5] They discussed the presence of super-cooled water to explain the results obtained. Tajiri et al.[6] and Mukundan et al.[4] investigated isothermal cold start. Tajiri used the amount of total product water in mg cm^{-2} during startup as an index to quantify cold-start capability, while Mukundan et al. used Coulombs transferred for a similar effect. Tajiri et al. found that the pore volume of the cathode catalyst layer is not fully utilized for ice storage at high current. Oszcipok et al.[7] conducted potentiostatic single-cell experiments. They used the calculated cumulative charge transfer through the membrane, which directly corresponds with the amount of produced water in PEFCs. They concluded that produced water increases the membrane water content first, and then floods the electrode, MPL and GDL, and freezes. Thompson et al.[8] used cryo-scanning electron microscopy to quantify the water holding content after voltage failure of PEFC after start-up at −20°C, and found that at low current densities the membrane absorbs a maximum of 14 to 15 water molecules per sulfonate group while at higher current densities the maximum charge storage is not utilized. Wang et al.[9] defined three stages of cold-start and explored the maximum ice accumulation and cell voltage variations during cold start. They also experimentally determined the ionic conductivity of Nafion 117 under subfreezing condition, showing that a portion of water freezes in the membrane which contributes little to ionic conductivity. Hiramitsu[10] examined the role of the ionomer/carbon ratio in the catalyst layer from 0.5 to 1.5, finding that higher ionomer content improved cold start performance because of better oxygen permeation in the catalyst layer. Chacko et al.[11] studied cold start at −10°C, and found that a dry membrane leads to better cold start because there is more space for water storage in the membrane, thus the high frequency resistance (HFR) initially decreases.

Modeling studies of cold-start have also been reported. Wang[12] analyzed water transport, ice formation, and the mechanisms of ice impact on cell voltage under cold start. The time constants of several important processes during cold start were analyzed. Ahluwalia and Wang[13] developed a two-dimensional model of a single cell for simulating PEFC cold-start in order to determine conditions necessary for successful cold startup. They found that there exist critical temperatures beyond which self-startup is not possible, and found that due to low thermal mass preheating reactant flows has minimal effect, while thinner bipolar plates and isolation of stack coolant are beneficial. Mao and Wang presented one of the first multiphase models[14] to study PEFC cold start, based on the three-dimensional transient formulation of PEFCs developed by Wang and Wang.[15] Meng[16] investigated the impact of several parameters on isothermal cold-start behaviors, indicating that high gas flow rate, low initial membrane water content, low current density, and high cell voltage are beneficial to cold start. Ko and Ju[17] developed a multiphase transient model to look at the effects of catalyst-layer composition on cold start, including Pt loading and CL thickness. Balliet and Newman[18] presented a two-dimensional cold start model which they then used to predict results for ultrathin cathode catalyst layers. They suggest fuel cells with ultrathin cathode catalyst layers could be started with a drier membrane, or at lower potential.

Though experimental studies have been carried out previously, there are several aspects that are still not fully understood in subfreezing operation: the effects of electrode configuration (such as thickness and the IC ratio), the effects of membranes (such as thickness and initial hydration state), the effects of various operating conditions (such as subfreezing temperature and current densities), and most importantly their comparison. In this study, we experimentally investigated these important parameters, and use the concept of coulombs of charge Q_c transferred before operational failure as an index by

*Electrochemical Society Active Member.
[z]E-mail: yunw@uci.edu

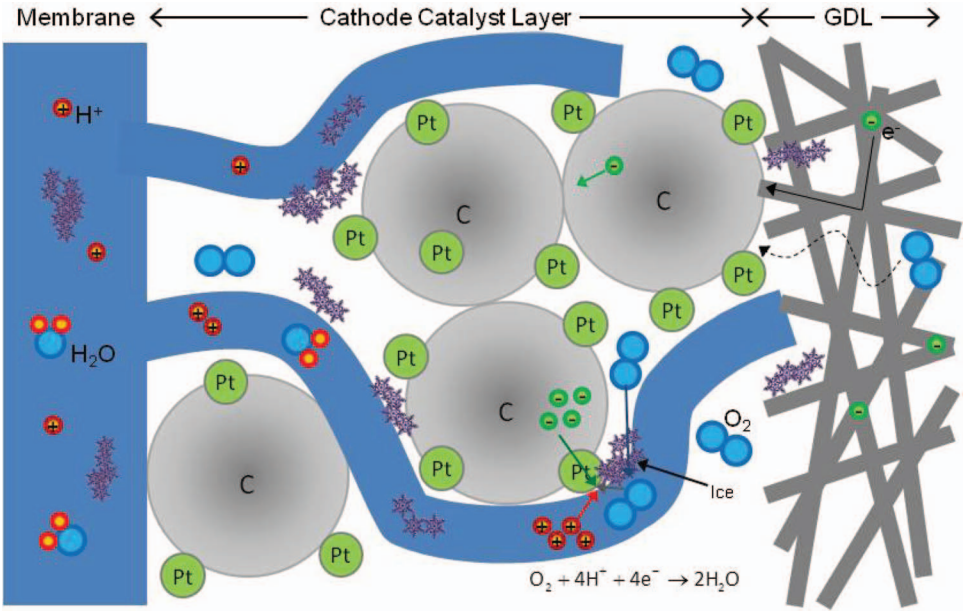

Figure 1. Schematic of ice production and storage within the cathode catalyst layer.

which we characterize the cold-start performance. Q_c quantifies both the ice holding capacity and the amount of waste heat generated by PEFCs. Theoretical analysis was also performed to aid experimental explanation.

Experimental

All experiments were conducted in single-cell fuel cell hardware specially designed for cold start experiments. In addition to the quad-serpentine flow field for the reactants and products to enter and exit the fuel cell, cooling channels were fabricated and incorporated into the fuel cell hardware. Temperature control was maintained by use of heating cartridges during normal operating conditions (80°C), and circulating cooling fluids during subfreezing operating conditions with a thermocouple close to the edge of the bipolar plates. Figure 2 shows the construction of the experimental fuel cell.

Different membrane electrode assemblies (MEA) were constructed in order to study the key variables in the MEA design for cold-start concerns. The catalyst layer was fabricated with catalyst inks made of platinum supported on Vulcan XC-72 carbon black and Nafion ionomer. Different Pt/C catalysts were mixed with a 5% Nafion solution, and then tetrabutylammonium hydroxide (Bu_4NOH, or TBAOH) and glycerol were added. The ink was painted onto decals to a loading to 0.2 mg Pt/cm^2 on both the anode and cathode sides and dried until only the Pt/C catalyst and Nafion ionomer remained. The catalyst layers were transferred onto the membranes by hot-pressing them at 210°C for 5 minutes.[19]

Nafion membranes of two different thicknesses (1 and 2 mil, or 25 and 50 μm) were tested with ink composed of 20 wt%Pt on carbon black (cell #1 and cell #2). The thickness of the catalyst layer was controlled by means of altering the concentration of platinum on carbon from 20% to 40% (cell #3). Lastly the ionomer to carbon

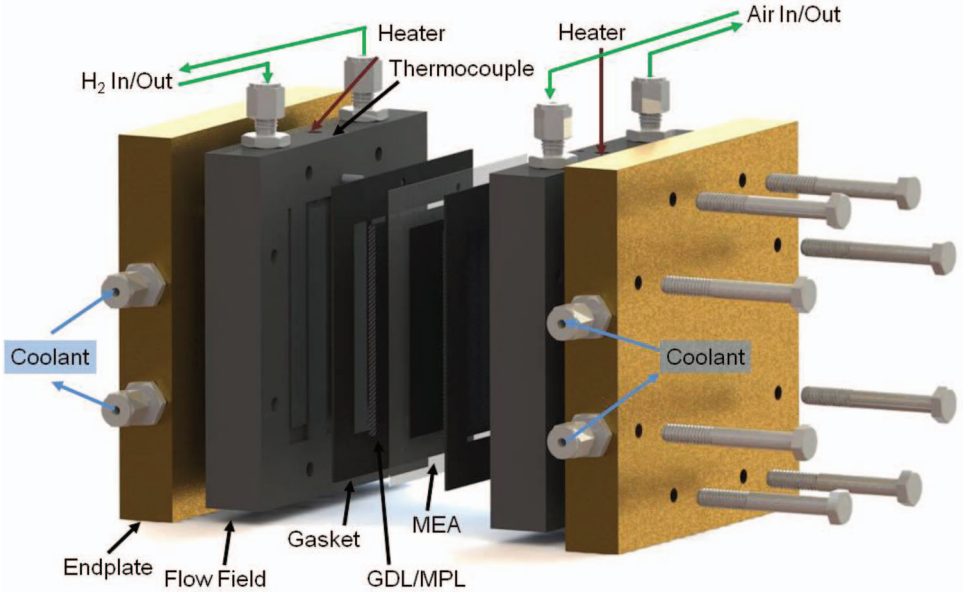

Figure 2. Schematic of the PEFC designed for cold-start experiments.

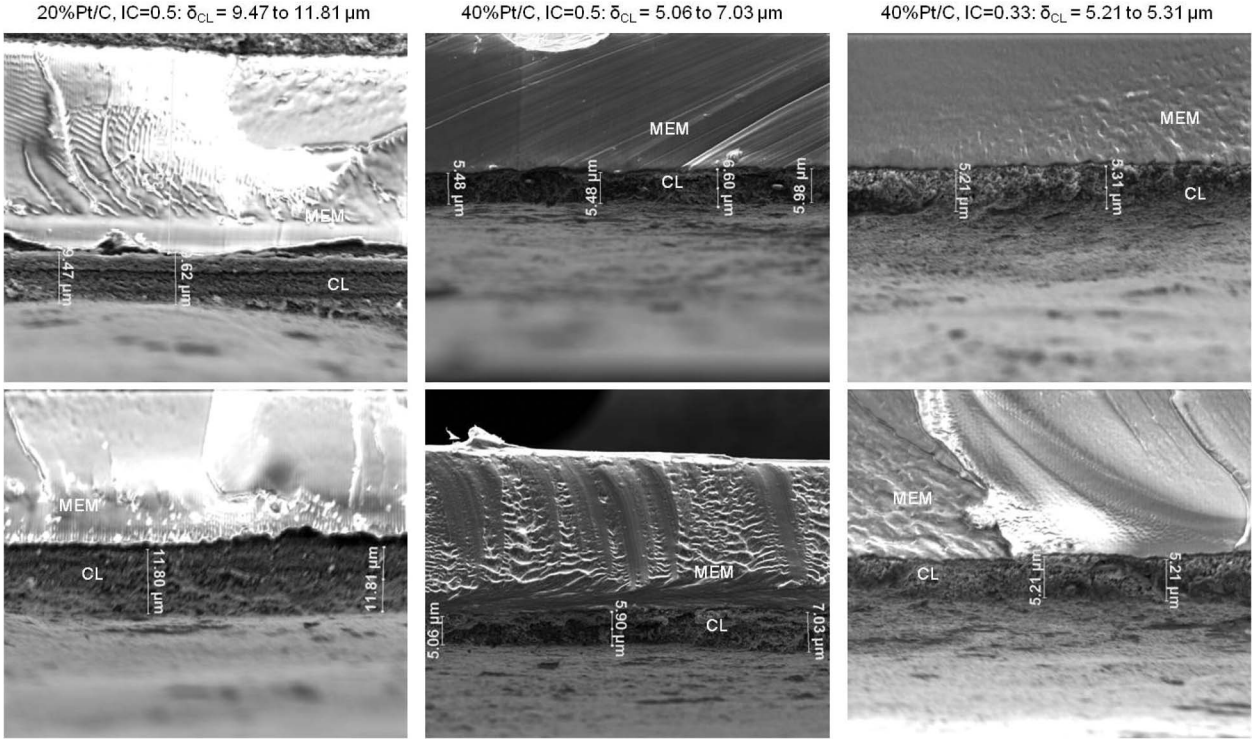

Figure 3. SEM images of catalyst layers: 20%Pt/C, I/C ratio of 0.5 (left) and 40%Pt/C, I/C ratio of 0.5 (center) and 0.33 (right). Each is measured at two different locations.

black ratio (I/C ratio) within the catalyst layer was altered between 0.33, 0.5, and 0.66 (cell #4, cell #3, and cell #5). Changing the I/C ratio yields different thicknesses of catalyst layers at given Pt loading. Figure 3 shows the scanning electron microscope (SEM) images of three catalyst layers tested in this study. From left to right it shows the 20 wt%Pt with I/C ratio of 0.5, 40 wt%Pt with the I/C ratios of 0.33 and 0.5, respectively. The thickness is not uniform throughout the catalyst layer (CL), as a result of the fabrication process, thus multiple measurements of thickness were taken in order to get a range of thicknesses. It can be seen that the 20 wt%Pt CL is about two-times thicker than that of the 40 wt%Pt CL. Additionally, Figure 3 shows that the catalyst layer of the 0.5 ratio is thicker than that of 0.33: for the former the thickness varies from 5.06 μm to 7.03 μm with an average around 6.00 μm, whereas for the latter it changes from 5.21 μm to 5.31 μm. Note that the catalyst layer thickness plays an important role in cold start, which was studied in this experiment. A summary of the MEA and catalyst-layer compositions are presented in Table I, and the dimensions and operating conditions of the PEFC are presented in Table II. The fuel cell was assembled with SGL SIGRACET 24BC GDLs of a nominal thickness of 235 μm,[20] and polyurethane gaskets. The flow field is quad serpentine with an active area of 50 cm^2.

The fuel cells were first conditioned and run overnight at 80°C and 0.6 V to establish baseline performance. They were run at the stoichiometric flow ratios of 1.2 and 2.0 for the anode and cathode, respectively, and at 1 atm absolute pressure with 25 psi back pressure. The fuel cells were then prepared for testing by running them at 0.6 V with inlet gas flows at a specific relative humidity (RH), either 100% or 50%. The high frequency resistance was measured while running under these conditions. The current was then reduced to zero and both sides of the cell were purged with dry nitrogen at 1 L/min for 2 minutes. After the gas purge the temperature was reduced to sub-zero using coolant flows, either to −10°C or −20°C. The fuel cell was then operated isothermally at a sub-freezing temperature and 0.02, 0.04, or 0.08 A/cm^2, with a high stoichiometry of dry H_2 and air, 500 sccm. The voltage was monitored during this time, and the current was turned off once the fuel cell reached voltage failure, defined as reaching 0.0 V. The testing was halted when the voltage first showed a negative value, which indicted the fuel cell could no longer produce the imposed current. The time of failure was taken as the time stamp of the recording just before the negative voltage reading. High frequency resistance (HFR), current transferred, and cell voltage evolution were measured during each test. The fuel cell was then heated up to 80°C

Table I. Membrane and catalyst layer configurations.

Cell #	Membrane	Ink (0.2 mg/Pt cm^2 both sides)	Ionomer-Carbon Ratio (IC)*
1	NR-211	20%Pt/C Ink	0.5
2	NR-212	20%Pt/C Ink	0.5
3	NR-212	40%Pt/C Ink	0.5
4	NR-212	40%Pt/C Ink	0.33
5	NR-212	40%Pt/C Ink	0.66

*IC ratio: the weight ratio of ionomer to carbon-black in the ink.

Table II. PEFC dimensions and operating conditions.

Parameters	Values
MEA size	50 cm^2
Bipolar plate	Graphite, quad serpentine
Channel dimension	0.04 mm × 0.04 mm
Rib dimension	0.04 mm
Pt loading	0.2 mg/cm^2
wt% Pt on Carbon black	20 wt%, 40 wt%
GDL	SGL SIGRACET 24BC GDL
PTFE loading	5% GDL substrate, 23% MPL
Gas flow rate during cold start	500 sccm
Pressure	25 psi back pressure
Temperature	−10°C, −20°C
Pre-freeze inlet flow RH	50%, 100%
Current density of sub-freezing operation	0.02, 0.04, 0.08 A/cm^2

and again run at 0.6 V and given humidity to prepare for the next test. This was repeated for 12 test conditions (i.e. three current densities, two subfreezing temperatures, and two RH conditions) per fuel cell. The coulombs of charge was calculated using Eq. 3 (to be presented in the next section), i.e. the duration of operation under the constant current times the current density. Given the time resolution of data acquisition was 0.001 hr, or 3.6 seconds, the uncertainty in the recorded amount of coulombs is 0.072, 0.14, and 0.29 C/cm^2 for 0.02, 0.04, and 0.08 A/cm^2, respectively.

$$\int_0^{\tau_{T,1}} (E_o - V cell)dt = \frac{(m_m Cp_m + m_{CL} Cp_{CL} + m_{GDL} Cp_{GDL} + m_{BP} Cp_{BP})(273.15 - T_o)}{A_m I} \quad [5]$$

Coulombs of charge transferred before operational failure.— Ice holding capability is defined as how much ice a fuel cell can hold before ice terminates its operation, and can be quantified in terms of volume of ice, or equivalently in terms of charge transferred in the production of that ice, as we do in this study. This capacity can then be compared to the amount of charge required to produce enough heat to raise the temperature of the fuel cell above the freezing point, as shown later in this section.

Under constant current density, the capacity can be quantified using the time constant of ice formation inside the cathode catalyst layer, assuming that ice formation in this component is the cause for PEFC shut-down. The time duration for the ice volume fraction in the cathode catalyst layer to reach 1 was derived as:[12]

$$\tau_{s_{ice}} = \tau_{ice,1} + \tau_{ice,2} = \frac{2F\delta_{CL}}{(1+2\alpha)I}\left[\frac{\rho_m \varepsilon_m(\lambda_{sat} - \lambda_o)}{EW} + \frac{\rho_{ice}\varepsilon_{CL}}{M^W}\right] \quad [1]$$

where

$$\tau_{ice,1} = \frac{2F\rho_m\varepsilon_m\delta_{CL}(\lambda_{sat} - \lambda_o)}{EW(1+2\alpha)I} \quad \text{and} \quad \tau_{ice,2} = \frac{2F\rho_{ice}\varepsilon_{CL}\delta_{CL}}{(1+2\alpha)M^W I} \quad [2]$$

where EW is the equivalent weight of the dry membrane, α is the net water flux per proton flux through the membrane, F is Faraday's constant, M^W is the molecular weight of water, and ρ_m and ρ_{ice} are the densities of the membrane and of ice, respectively. A number of material properties and operating parameters affect this duration, including the catalyst layer thickness δ_{CL}, membrane initial/saturated water content λ_0/λ_{sat}, the ionomer volume fraction in the catalyst layer ε_m, the porosity ε_{CL}, and constant current density I. Herein, the definition of α can be extended to represent the net water transport into the cathode catalyst layer, i.e. the water entering the cathode GDL, if any, will be counted as water loss for the cathode catalyst layer. The two time constants characterize water holding capacity in the ionomer phase $\tau_{ice,1}$ and ice holding capacity in the void space $\tau_{ice,2}$ of the cathode catalyst layer. In addition, the amount (or coulombs) of charge Q_c produced is defined as:

$$Q_c = \int_0^{\tau} I(t)dt \xrightarrow{I=const} Q_c = I\tau \quad [3]$$

where τ is the time constant for operation failure. Our experiments were run at constant current I. In the experiment, we used Eq. 3 to obtain Q_c. Note that Q_c is proportional to the water production rate, given by Faraday's law, thus it characterizes the amount of ice produced in a PEFC at subfreezing condition.

For analytical purposes, we can assume $\tau = \tau_{s_{ice}}$. To explicitly show Q_c at subfreezing condition, one can move the current density in Eq. 1 to the left side, yielding:

$$Q_c = \tau_{s_{ice}} I = (\tau_{ice,1} + \tau_{ice,2})I = \frac{2F\delta_{CL}}{(1+2\alpha)}\left[\frac{\rho_m\varepsilon_m(\lambda_{sat} - \lambda_o)}{EW} + \frac{\rho_{ice}\varepsilon_{CL}}{M^W}\right] \quad [4]$$

It is seen that the amount of coulombs is determined by a number of parameters. As α depends on operation conditions, Q_c changes from case to case.

During cold start, ice formation competes with cell temperature increase as a result of the waste heat generated by the PEFCs reactions or any external heat addition. In the simplest scenario in which no external heat sources are presented, a time constant $\tau_{T,1}$ can be derived to characterize PEFC's overcoming the freezing barrier, i.e. 0°C, as follows:[9]

To obtain a more simplified expression, we approximate the PEFC's thermal mass by the thermal mass of its bipolar plates $m_{BP}Cp_{BP}$, provided that the latter is much larger than the rest, and assume a constant cell voltage:

$$\tau_{T,1} = \frac{\rho_{BP}Cp_{BP}\delta_{BP}}{I(E_o - V cell)}(273.15 - T_o) \quad [6]$$

Because this time constant gives the duration for the PEFC to overcome the cold-start barrier, another quantity, the coulombs of charge $Q_{c,\min}$, in cold start can be defined by moving the current density to the left side:

$$Q_{c,\min} = I\tau_{T,1} = \frac{\rho_{BP}Cp_{BP}\delta_{BP}}{(E_o - V cell)}(273.15 - T_o) \quad [7]$$

This amount of coulombs characterizes the minimum amount of charge needed to successfully heat the cell to T > 0°C in a cold start.

Following Wang,[12] a parameter can be defined by using the concept of coulombs of charge:

$$\beta_2 = \frac{\tau_{T,1}}{\tau_{s_{ice}}} = \frac{I\tau_{T,1}}{I\tau_{s_{ice}}} = \frac{Q_{c,\min}}{Q_c} \quad [8]$$

For $\beta_2 > 1$, cold start will fail. In this work, experiment is designed at constant subfreezing temperature, in which the waste heat is taken away by cooling flow (or in another words, $Q_{c,\min} \to \infty$). Thus, PEFC operation will eventually fail.

Results and Discussion

The performance of each of the fuel cells at normal operating conditions of 80°C and 100% RH inlet flows is shown in Figure 4. At 0.6 V, the two fuel cells with the 20%Pt/C catalyst have a current density of over 1.2 A/cm^2, in which at 0.4 V the cell with the thinner NR211 membrane reaches 1.95 A/cm^2. It is seen that the catalyst configuration and thickness as well as the membrane thickness affect fuel cell performance under normal conditions. Below, we examine the subfreezing operation of the fuel cells.

A successful cold start has three stages, as defined by Wang[9]. By this experimental design, the iso-thermal subfreezing operation experiences only the first two stages. The left side of Figure 5 shows the voltage evolution until fuel cell failure, while the right side plots the high frequency resistance (HFR) during the same time period. In the first stage, product water hydrates the membrane phase, as seen in the schematic in Figure 1, therefore increasing the ionic conductivity and decreasing the ohmic loss. This is observed as a decrease in the HFR and a corresponding slight increase in the cell output voltage in Figure 5. The time constant $\tau_{ice,1}$ gives the duration of this stage. The second stage of cold startup is the ice formation in void space. Ice begins to form in the cathode catalyst layer, hampering oxygen transport and reaction activity. Ice formation eventually causes operational failure. There is a considerable increase in the concentration

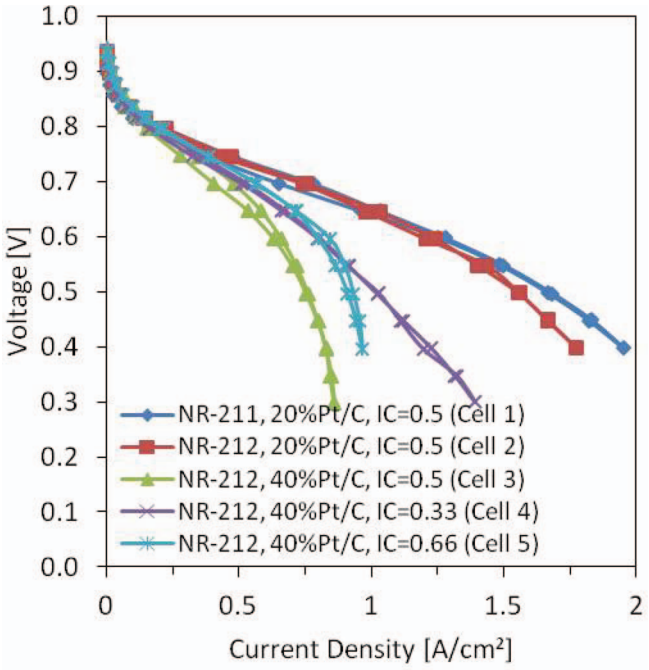

Figure 4. Voltage-Current curves for all of the tested fuel cells. Curves are shown for operation at 80°C, 100% RH inlet flows. NR-211 and NR-212 refer to Nafion membranes of thickness 1 and 2 mil (25 and 50 μm), IC is ionomer to carbon ratio.

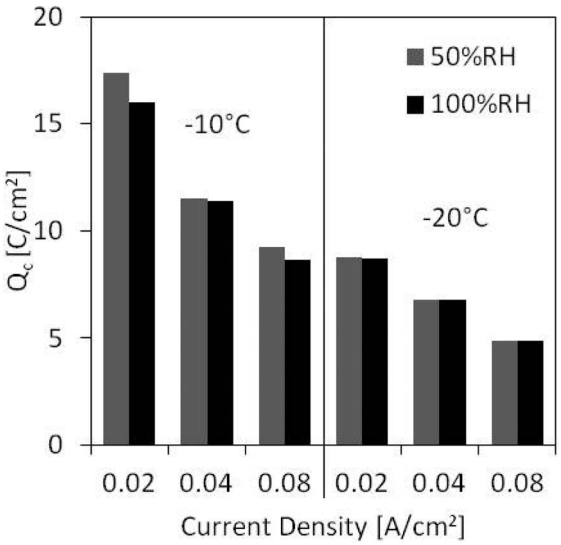

Figure 6. Coulombs transferred before voltage failure at current densities of 0.02, 0.04, 0.08 A/cm^2 and temperatures of −10°C and −20°C for cell #1.

overpotential seen graphically by the quick decrease of voltage near operation failure in Figure 5. The time constant $\tau_{ice,2}$ in Eq. 2 characterizes the duration of this stage. In this stage, most produced water is in solid ice phase, and does not necessarily diffuse into the membrane to compensate for its water loss due to the electro-osmotic drag, leading to an increase in the HFR. The third stage of cold start is when the waste heat produced by the reaction melts ice at 0°C. In our experiments, PEFCs were kept at constant temperature by using cooling flow. Thus the PEFCs do not experience this third stage of cold start.

Effect of operating conditions.— Operating conditions affect the timing of voltage failure. Figure 6 shows the coulombs of charge transferred in cell #1 before voltage failure for the initial state at 50% RH. The amounts of charge were calculated by multiplying the operating time by the experimental current density, i.e. Eq. 3. In addition to earlier failure at higher currents, as shown in Figure 5, the total amount of charge transferred decreases. This is due to the longer operating duration at lower current density, which allows more water in the cathode to be transported to the regions of the membrane, GDL, and even anode, thus increasing the ice holding capacity of the fuel cell. From Eq. 4, it is clear that smaller α yields increased Q_c. In addition, higher current operation exhibits larger voltage loss, thus earlier operation failure (or the cell voltage reaches 0.0 V earlier).

In addition, the 50% RH case has a higher starting HFR as shown in Figure 7, indicating less hydration in the membrane, i.e. a lower value of λ_0. Drier membranes have more capability to hold water before reaching saturation. In the catalyst layer, there is a small portion of Nafion ionomer phase, which at a dry state absorbs water when extra water is added through the ORR. Though the water holding capacity in the electrolyte membrane is large as indicated by Wang and Wang,[15] that of the catalyst layer is small because of its thickness (<15 μm) and small volume fraction of ionomer (usually <0.4). Wang[12] evaluated the hydration timescale by assuming a value of 14 as saturated water content in the ionomer phase, showing in a case that for 0.1 A/cm^2 it takes around 5 seconds, as opposed to that (∼30 seconds) for the ice formation in void space. Figure 6 shows that more coulombs are transferred for the drier case, 50% RH, than the 100% one, at −10°C, as expected. Eq. 4 also shows smaller λ_0 yields larger Q_c. However, no difference was observed for −20°C between these two RHs, as shown in Figure 6. This may be partly due to the fact that a portion of water freezes in the membrane phase at subfreezing temperature. Wang et al. showed that the ionic conductivity changes little when water content is over around 7.22 or the water activity of 0.8. They ascribed it to the frozen water in the membrane, which contributes little to ion transport.

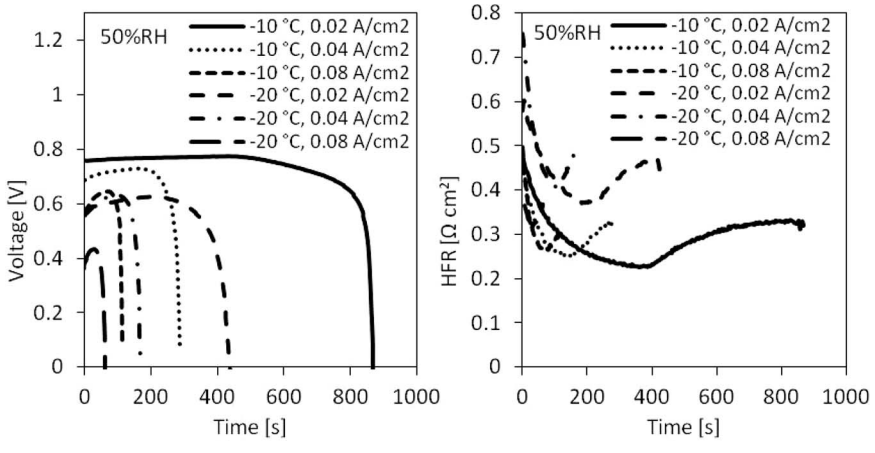

Figure 5. The voltage (left) and HFR (right) evolution of cell #1 under subfreezing operation for the initial state at 50% RH.

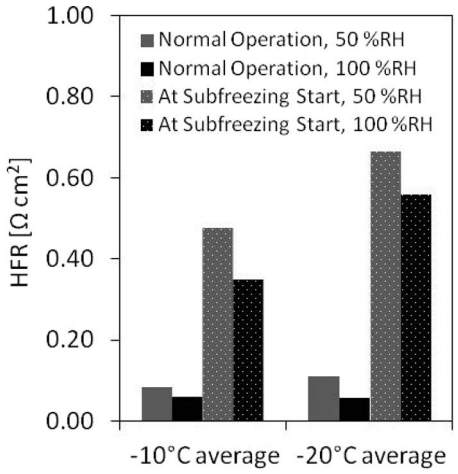

Figure 7. The HFRs (high frequency resistance) of cell #1. The solid colored bars represent the HFR at 80°C, and the dotted bars show the HFR at the beginning of subfreezing operation.

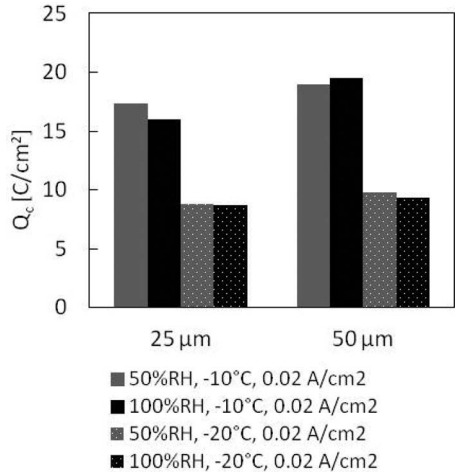

Figure 9. Coulombs transferred before failure for fuel cells with different membrane thicknesses, cells #1 and #2. Both fuel cells have a catalyst layer composed of 20 wt% Pt/C, IC = 0.5.

It could be true that at lower temperatures more water in the membrane tends to freeze. Thus, for −20°C no obvious difference was observed between the two RHs, as a result of the membrane phase being nearly saturated with non-frozen water at the 50% RH. In another words, in Eq. 4, the value of λ_{sat}-λ_0 may be close to zero for the two cases at −20°C, yielding similar Q_c. In addition, given only a small portion of the Nafion ionomer present in the catalyst layer, its storage effect can be small. The water diffusivity at −20°C is also weaker than that of −10°C, yielding less water storage by the membrane. Furthermore, the 50% RH presents a higher membrane resistance and hence larger ohmic loss. The larger ohmic loss shortens the duration of voltage drop to 0.0 V, which may be another reason for the little difference observed between the two RHs at −20°C. Again from Figure 6, it is seen PEFCs may not be able to take full advantage of the extra water storage space within the dry membrane phase around −20°C or lower for the studied membrane and humidification condition.

Figure 7 shows the HFRs in PEFCs at 80°C and at the beginning of cold start, respectively. It can be seen that there is a dramatic increase in the HFR when temperature changes from 80°C to the freezing temperatures. This increase arises from the temperature dependence of the ionic conductivity and likely of the contact resistance among components. In addition, the HFR at 50% RH is higher than that of 100% RH at both temperatures, showing that a better hydrated membrane exhibits higher ionic conductivity. Contact resistance may contribute to the observed HFR increase, as a result of the thermal expansion of PEFC components.

Effect of membrane thickness and catalyst layer configuration.— The next step in our testing was to examine the effects of MEA properties on coulombs of charge transferred. Towards this goal, we used Nafion membranes of different thicknesses and catalyst layers of different I/C ratios and thicknesses. The voltage and HFR evolutions for −10°C, 0.02 A/cm^2 and initial state at 100% RH are shown in Figure 8. All the cases show a similar trend as in Figure 5: a gradual change in cell voltage, followed by a rapid drop. It is clear that MEA properties affect the timing of operation failure and hence the coulombs of charge transferred.

Figure 9 shows the coulombs of charge for the fuel cells with the NR211 and NR212 membranes, respectively. These are Nafion membranes which have a thickness of 1 mil and 2 mil (25 µm and 50 µm), respectively. For each tested condition the thicker NR212 membrane sustained the operating current for longer, indicating that part of the produced water was stored in the membrane. However, the difference between them is small. The sluggish diffusion of water at subfreezing temperature limits the ability to fully utilize the storage space in the thicker membrane. For the thicker membrane, it is observed that the 100% RH case shows a slightly higher value of coulombs than that of 50% RH at −10°C. This may be caused by the high ohmic resistance in the 50% RH case, which led to an early stage of output voltage dropping to 0 V. For the thinner membrane, the ohmic resistance becomes smaller, and may have limited effect on shortening the operating time, thus the 50% RH case shows a larger amount of charge than the 100% RH. As to −20°C, more water may freeze in the membrane. Thus,

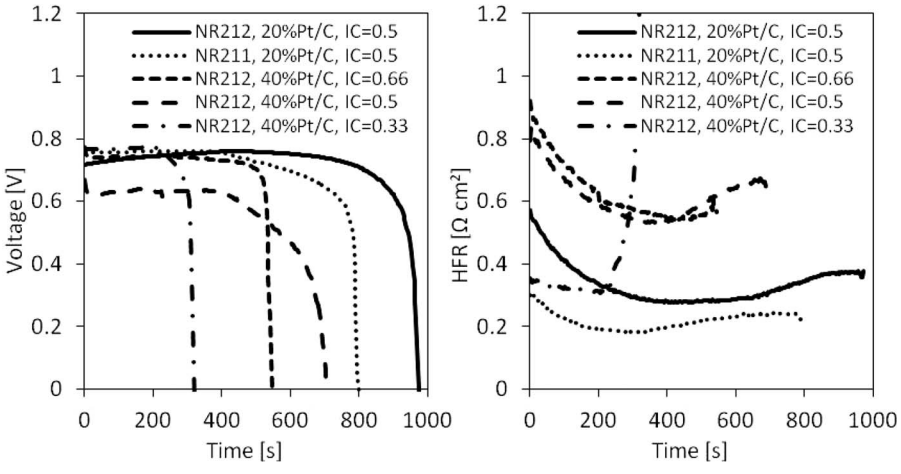

Figure 8. The voltage (left) and HFR (right) evolution for all of the tested cells at −10°C, 100% RH, and 0.02 A/cm^2.

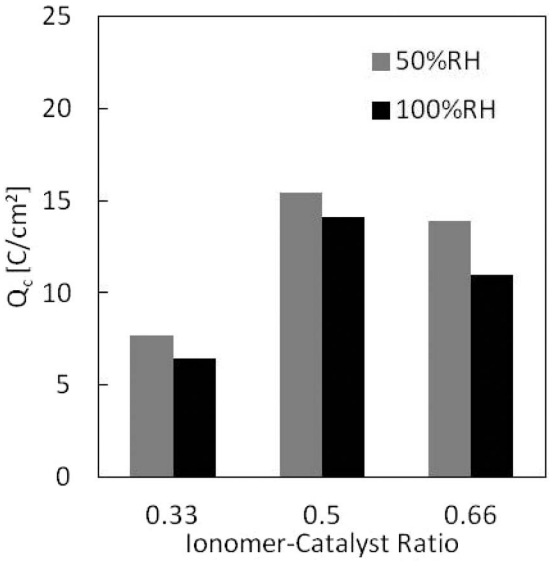

Figure 10. Charge transferred before voltage failure for cells #3-5 under -10°C and 0.02 A/cm^2.

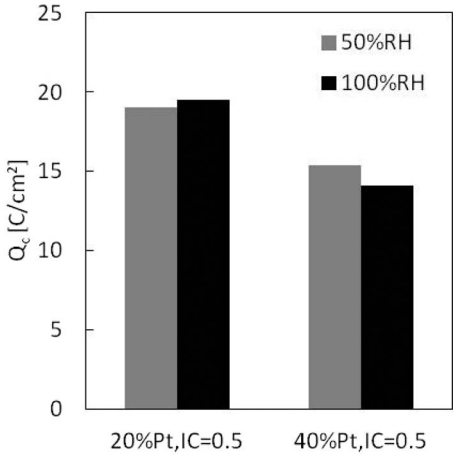

Figure 11. Coulombs of charge transferred before operation failure for 20 and 40 wt% Pt on Carbon black, respectively, for cells #2 and #3 under -10°C and 0.02 A/cm^2.

the ohmic resistances become closer between 50% and 100% (as also shown in Figure 7). As a result, the 50% RH case exhibits slightly larger coulombs of charge transferred than 100% RH for the thicker membrane.

Two variables are studied with respect to the catalyst-layer configuration. The first is the weight ratio of ionomer to carbon (I/C). The ratio was varied between 0.33, 0.5, and 0.66, see Table I for cell configurations. Figure 10 shows the coulombs of charge transferred before operation failure at 0.02 A/cm^2. Q_c increases when the I/C ratio changes from 0.33 to 0.5, but decreases when the IC ratio moves from 0.5 to 0.66. For the former observation, increasing the amount of ionomer gives more space for water to be held (see Figure 3: the 0.5 I/C ratio shows a slightly thicker catalyst layer than that of 0.33), and also allows for more water back-diffusion to the membrane. In the work of Hiramitsu,[10] the I/C ratios of 0.5, 1.0, and 1.5 were examined at higher current densities, and found that more ionomer enables the fuel cells to last longer before failure. Our study shows a tradeoff for the I/C ratio, likely a tradeoff between the CL void space's ability to store water and deliver oxygen reactants, and the CL ionomer content's ability to store water and transport water to the membrane. From Eq. 4, it is clearly shown that both ε_m and ε_{CL} affect Q_c. Changing the I/C ratio affects both parameters: increasing ε_m will likely reduce the value of ε_{CL}.

The catalyst layers of two thicknesses δ_{CL} were fabricated. In both thicknesses, we keep the I/C ratio and the Pt loading constant at 0.5 and 0.2 mg/cm^2, respectively, and changed the Pt/C weight ratio, thus, the 40 wt% Pt/C catalyst layer has a thickness that is about half of the 20 wt% one. Figure 11 compares the two catalyst layers, on the left having 20 wt% Pt/C, and on the right having 40 wt%. It is seen Q_c is larger for the thicker catalyst layer than that of the thinner one, because the extra space for storing ice in the thicker layer. This can be clearly seen from Eq. 4, showing a thicker δ_{CL} yields a larger Q_c. In addition, for the 20 wt% Pt/C or thicker CL case, 100% RH shows a larger capacity of charge. This is likely due to the spatial variation of reaction: for 50% RH a higher ionic resistance is present in the catalyst layer, leading to a larger value of non-homogeneity factor $\hbar$ ($= \frac{\Delta U}{2R_gT/\alpha_c F}$ where $\Delta U = \frac{I\delta_{CL}}{\sigma_m^{eff}} = I R_\delta$). Wang and Feng [21] showed that more local reactions occur near the interface between the membrane and catalyst layer, thus the oxygen transport polarization is more severe. As to 100% RH, the reaction is more uniform than that of 50% RH, leading to less polarization of oxygen transport. It is likely that the severe polarization of oxygen transport in 50% RH shortens the period of time for output voltage to drop to 0 V, leading to the observed less coulombs of charge. For the 40 wt%, the catalyst layer's thickness is about half, and oxygen transport resistance across the layer is less important, thus the 50% RH case shows a larger amount of charge transferred than the 100% RH case.

Conclusions

In this paper, we fabricated PEFCs and experimentally investigated their subfreezing performance under different membrane, catalyst layer thicknesses, IC ratios in the catalyst layers, hydrated conditions, and temperatures. Coulombs of charge transferred Q_c was introduced to characterize PEFC subfreezing operation. We found that:

- Under lower current densities, the PEFCs exhibited larger Q_c, which is due to two reasons: longer operation duration that enables more product water to transport to the membrane, and the smaller voltage loss. Q_c at 0.02 A/cm^2 is ~50% larger than that of 0.08 A/cm^2.
- Under lower temperature, the PEFCs showed smaller Q_c, and a 55% reduction was observed from -10°C to -20°C at 0.02 A/cm^2 for an I/C of 0.5 and Nafion 211.
- The effect of membrane thickness on Q_c was found to be relatively small. The water storage capability of membranes was not fully utilized for the studied RH conditions.
- The effect of the initial membrane hydration state on Q_c was found to be relatively small, particularly at -20°C.
- A thicker catalyst layer showed longer operation time and a larger Q_c, due to more space available for ice storage in the catalyst layer.
- The I/C ratio of 0.5 was found to exhibit the largest Q_c.

The results show that MEA design and vehicle start-up strategies can be optimized for freezing operation, and findings are significant to PEFC vehicular applications.

Acknowledgments

The authors express their thanks to all those who assisted in the writing of this paper. This work was supported by the Fuel Cell Technologies Program at the U.S. Department of Energy - Energy Efficiency and Renewable Energy, Technology Development Manager: Nancy Garland.

References

1. Y. Wang, K. S. Chen, J. Mishler, S. C. Cho, and X. C. Adroher, *Applied Energy*, **88**, 981 (2011).

2. Hydrogen, Fuel Cells & Infrastructure Technologies Program Multi-Year Research, Development and Demonstration Plan. 14 Table 13.14.12 (US DOE EERE, 2007).
3. J. Mishler, Y. Wang, P. P. Mukherjee, R. Mukundan, and R. L. Borup, *Electrochimica Acta*, **65**, 127 (2012).
4. R. Mukundan et al., *ECS Transactions*, **25**, 345 (2009).
5. P. Oberholzer et al., *Journal of The Electrochemical Society*, **159**, B235 (2011).
6. K. Tajiri, Y. Tabuchi, and C.-Y. Wang, *Journal of The Electrochemical Society*, **154**, B147 (2007).
7. M. Oszcipok, D. Riemann, U. Kronenwett, M. Kreideweis, and M. Zedda, *Journal of Power Sources*, **145**, 407 (2005).
8. E. L. Thompson, J. Jorne, W. Gu, and H. A. Gasteiger, *Journal of The Electrochemical Society*, **155**, B625 (2008).
9. Y. Wang, P. P. Mukherjee, J. Mishler, R. Mukundan, and R. L. Borup, *Electrochimica Acta*, **55**, 2636 (2010).
10. Y. Hiramitsu, N. Mitsuzawa, K. Okada, and M. Hori, *Journal of Power Sources*, **195**, 1038 (2010).
11. C. Chacko, R. Ramasamy, S. Kim, M. Khandelwal, and M. Mench, *Journal of The Electrochemical Society*, **155**, B1145 (2008).
12. Y. Wang, *Journal of The Electrochemical Society*, **154**, B1041 (2007).
13. R. K. Ahluwalia and K. Wang, *Journal of Power Sources*, **162**, 502 (2006).
14. L. Mao, C.-Y. Wang, and Y. Tabuchi, *Journal of The Electrochemical Society*, **154**, B341 (2007).
15. Y. Wang and C.-Y. Wang, *Electrochimica Acta*, **50**, 1307 (2005).
16. H. Meng and B. Ruan, *International Journal of Energy Research*, **35**, 2 (2011).
17. J. Ko and H. Ju, *International Journal of Hydrogen Energy* (2012).
18. R. J. Balliet and J. Newman, *Journal of The Electrochemical Society*, **158**, B939 (2011).
19. M. S. Wilson and S. Gottesfeld, *Journal of The Electrochemical Society*, **139**, L28 (1992).
20. SGL. *Sigracet GDL 24 & 25 Series Gas Diffusion Layer*, http://www.fuelcellmarkets.com/content/images/articles/GDL_24_25_Series_Gas_Diffusion_Layer.pdf.
21. Y. Wang and X. Feng, *J. Electrochem. Soc.*, **156**, B403 (2009).